chemengineering

MDPI

Article

MnO_2-Coated Dual Core–Shell Spindle-Like Nanorods for Improved Capacity Retention of Lithium–Sulfur Batteries

Hamza Dunya [1,2], Maziar Ashuri [3], Dana Alramahi [1], Zheng Yue [1], Kamil Kucuk [4], Carlo U. Segre [4] and Braja K. Mandal [1,*]

1 Department of Chemistry, Illinois Institute of Technology, Chicago, IL 60616, USA; hdunya@hawk.iit.edu (H.D.); dalramah@hawk.iit.edu (D.A.); zyue1@hawk.iit.edu (Z.Y.)
2 Department of Biotechnology, Bartin University, Bartin 74100, Turkey
3 Department of Mechanical, Materials, & Aerospace Engineering, Illinois Institute of Technology, Chicago, IL 60616, USA; mashuri@hawk.iit.edu
4 Department of Physics & Center for Synchrotron Radiation Research and Instrumentation (CSRRI), Illinois Institute of Technology, Chicago, IL 60616, USA; kkucuk@hawk.iit.edu (K.K.); segre@iit.edu (C.U.S.)
* Correspondence: mandal@iit.edu; Tel.: +1-312-567-3446; Fax: +1-312-567-3494

Received: 3 May 2020; Accepted: 18 June 2020; Published: 19 June 2020

Abstract: The emerging need for high-performance lithium–sulfur batteries has motivated many researchers to investigate different designs. However, the polysulfide shuttle effect, which is the result of dissolution of many intermediate polysulfides in electrolyte, has still remained unsolved. In this study, we have designed a sulfur-filled dual core–shell spindle-like nanorod structure coated with manganese oxide (S@HCNR@MnO_2) to achieve a high-performance cathode for lithium–sulfur batteries. The cathode showed an initial discharge capacity of 1661 mA h g^{-1} with 80% retention of capacity over 70 cycles at a 0.2C rate. Furthermore, compared with the nanorods without any coating (S@HCNR), the MnO_2-coated material displayed superior rate capability, cycling stability, and Coulombic efficiency. The synergistic effects of the nitrogen-doped hollow carbon host and the MnO_2 second shell are responsible for the improved electrochemical performance of this nanostructure.

Keywords: Lithium–sulfur batteries; manganese oxide; MnO_2 shell; sulfur; polysulfide shuttle; scalable synthesis; dual core–shell structure

1. Introduction

The depletion of fossil fuels and environmental issues arising from CO_2 emissions will force humankind to find alternative, clean means to satisfy its energy needs [1]. Rechargeable batteries are a vital component of the solution and research in this field has been increasing throughout the world [2,3]. Rechargeable Li-ion batteries have dominated portable electronic devices and hybrid electric vehicles (HEVs) since first being introduced in 1991. However, their high cost and low energy density have inhibited the mass-scale production of electric vehicles (EVs). The main reason for not shifting from HEVs to EVs on the roads is that state-of-the-art technology cannot satisfy the requirements of long-mileage driving, because of its energy density limitation barriers [4].

Lithium–sulfur (Li-S) batteries are among the most promising electrochemical energy storage devices of the near future [5]. The low cost and natural abundance of sulfur as well as its high theoretical specific capacity (1675 mA h g^{-1}) makes it an attractive cathode material [6]. In addition, sulfur has a high energy density (2600 W h kg^{-1}) and is environmentally friendly for energy storage applications. However, the commercialization of Li-S batteries is hindered, primarily due to the insulating nature of sulfur (5×10^{-30} S cm^{-1}) and volume expansion of the active material (sulfur) during discharge due to

the polysulfide shuttle (PSS) effect. The PSS leads to loss of active material from the cathode and causes irreversible reactions between the PSS intermediates and the lithium metal anode, which results in low coulombic efficiency and short cycle life [7–9]. Upon discharge, the sulfur is reduced to high-order PSS intermediates Li_2S_n ($3 \leq n \leq 8$) with an approximately 80% volume expansion that promotes the loss of active material [10,11]. The large volumetric expansion occurring due to the density difference between sulfur (2.03 g cm^{-3}) and Li_2S (1.66 g cm^{-3}) pulverizes the active material and accelerates rapid decay [6,12,13]. Furthermore, volume expansion can lead to mechanical cracking and deposition of the active material outside the electrode, which also results in loss of capacity [11,14].

To overcome the limitations of the insulating nature of sulfur, an effective approach has been focused on using carbon-based materials as the sulfur host (e.g., porous carbon [15–18], carbon nanotubes [19–22], graphene–graphene oxides [23–27]), since they address many of the challenges associated with Li-S technology. Carbon-based host materials have garnered the most interest since carbon provides higher conductivity and a physical barrier towards PSS, and accommodates the volume change that occurs during expansion, hence enhancing the utilization of the sulfur [16,28]. However, significant migration of the lithium polysulfides (LiPSs) is observed with carbon-based hosts due to the weak interaction between the polar LiPSs and the nonpolar carbon, resulting in capacity decay upon long-term cycling [29]. Recent literature has shown that polar materials such as sulfides, hydroxides, metal oxides and polymers can be employed as host materials in order to trap LiPSs as well as significantly improve long-term cycling stability by offering higher efficiency of LiPS chemisorption [30–33]. However, these materials generally have low electrical conductivity, which can potentially lead to low coulombic efficiency [34,35]. Therefore, it is essential to design a host structure that combines polar materials with carbon, which potentially may offer good conductivity and suppress the migration of LiPSs [36–38]. Manganese oxide has attracted significant attention because of its easy preparation and high efficiency in trapping polysulfides [39–43]. For instance, Nazar and coworkers demonstrated how MnO_2 is considered to be a remarkable chemical inhibitor of LiPSs by mediating polysulfides through the conversion of thiosulfate to polythionate species [44,45].

In response to the abovementioned issues associated with Li-S batteries, we prepared MnO_2-coated dual core–shell spindle-like nanorods, denoted as S@HCNR@MnO_2. The conductive nitrogen-doped carbon shell enhances the electrical conductivity of the cathode, while the outer polar MnO_2 layer is known to suppress the LiPSs. The double coating layers help to physically and chemically constrain the LiPSs. Furthermore, the volumetric expansion of sulfur upon lithiation is contained inside the nanorods. This novel design leads to a higher capacity and rate retention compared to pristine sulfur cathodes. To our knowledge, no other research group have tried to prepare such composite nanorods for this purpose.

2. Materials and Methods

2.1. Materials

Iron(III) chloride hexahydrate (97%), tris(hydroxymethyl) aminoethane hydrochloride (99+%), dopamine hydrochloride (99%), ethanol, polyvinylpyrrolidone (PVP, M.W. 40,000), and sublimed sulfur (~100 mesh, 99.5%) were purchased from Alfa Aesar®; urea (99%), hydrochloric acid (HCl, 37%), and potassium permanganate ($KMnO_4$, 99+%) were purchased from Sigma-Aldrich®. All the reagents were used without further purification.

2.2. Preparation of Nitrogen-Doped Hollow Porous Carbon Nanorods (N-HCNRs)

In a typical synthesis process [46], β-FeOOH nanorods were synthesized by using 2.25 g of $FeCl_3.6H_2O$ and 2.4 g of urea dissolved in 50 mL deionized (DI) water. The solution was refluxed at 90–95 °C for 8 h and further centrifuged and washed with deionized water multiple times to ensure removal of chloride ions from the surface of the product. The product was dried at 60 °C overnight. 0.63 g of β-FeOOH was mixed with 0.42 g of dopamine in Tris-buffer (700 mL, 10 mM; pH 8.5) and

stirred at 50 °C for 24 h. The resultant product was collected by centrifuge and washed with DI water and ethanol, followed by drying at 60 °C overnight. Calcination was carried out in a tubular furnace under Ar flow at 400 °C for 2 h with a heating rate of 1 °C min^{-1}, followed by further treatment at 500 °C for 2 h with a heating rate of 5 °C min^{-1}. The obtained powder was labeled as Fe_3O_4@N-C nanorods. The Fe_3O_4 core was etched with 2 M HCl aqueous solution and the precipitated layer was separated by centrifuge followed by washing with DI water until the pH of solution was stabilized at about 7. The final product (N-HCNR) was collected and dried in a vacuum oven at 60 °C overnight.

2.3. Preparation of S@HCNR

The sulfur/carbon composite was prepared by the melt-diffusion method. Elemental sulfur was ground with N-HCNR at a weight ratio of 7:3 and transferred into a Teflon®-lined autoclave and sealed under Ar gas. The autoclave was heated at 155 °C for 12 h to obtain S@HCNR.

2.4. Preparation of S@HCNR@MnO_2

The as-synthesized S@HCNR was dispersed in aqueous solution containing 40 mg of PVP for 2 h by ultrasonication, and then the mixture was stirred at room temperature for 1 h. Then, 48 mg of $KMnO_4$ was added to the solution, and the mixture was sonicated and the solid product was air-dried at 60 °C overnight (S@HCNR@MnO_2).

2.5. Characterization

Information about the surface morphology and elemental composition of the samples was confirmed by Phenom™ ProX scanning electron microscope (SEM). The nitrogen adsorption tests were carried out by a two-channel Quantachrome® Nova 2200e. All samples were degassed at 200 °C for 12 h under vacuum prior to testing. The amount of sulfur content in each specimen was determined by heating about 4 g of the material to 400 °C for 1 h at a heating rate of 10 °C min^{-1} under the nitrogen atmosphere. The remaining sample was collected carefully and weighed with a 4-digit balance to determine the weight change.

2.6. Electrochemical Measurements

The composite cathode cells of S@HCNR and S@HCNR@MnO_2 were fabricated by using 80 wt.% of active material, 10 wt.% Super P carbon black, and 10 wt.% of polyvinylidene fluoride (PVDF) with an appropriate amount of N-methyl pyrrolidone (NMP) to reach a viscous slurry. The slurry was casted onto a carbon-coated Al foil current collector and dried at 60 °C overnight. The loading of active material was maintained as ~1 mg cm^{-2}. We expect that the active material volume percentage of about 50% and the remaining 50% volume of the electrode is occupied by porosity, binder, conductive diluents, etc. Considering the percentage of the sulfur and C/MnO_2 in the active material, we can expect 40 vol.% of sulfur and 10 vol.% C/MnO_2 in the electrode. The porosity volume percentage is also estimated at about 30%. The electrochemical performances of the sulfur cathodes were tested using CR2032-type coin cells with Li metal as both reference and counter electrodes. Celgard® porous membrane was used as the separator. The electrolyte solution was composed of 1.0 M lithium bis(trifluoromethanesulfonyl)imide (LiTFSI) in 1,2-dimethoxyethane (DME) and 1,3-dioxolane (DOL) (*v*/*v* = 1:1), with 2 wt.% of $LiNO_3$. A quantity of 27 µL of the electrolyte was added to each cell. The cells were assembled inside an Ar-filled glove box, where both water and oxygen levels were below 1 ppm. Galvanostatic charge–discharge testing was carried out with Neware® battery testers within a potential range of 1.7–2.8 V vs. Li^+/Li. The reported capacities were normalized based on the sulfur content of the samples.

3. Results and Discussions

Figure 1 shows a schematic illustration of the several steps involved in the synthesis of the S@HCNR@MnO_2 nanorods. The first step was involved with the preparation of the well-defined

β-FeOOH nanorods by hydrothermal method, which acted as a hard template. Then, a dopamine layer was formed around the nanorods through a polymerization reaction at 50 °C, followed by subsequent carbonization to generate a nitrogen-doped carbon shell on the surface of the iron oxide core (Fe_3O_4@N-C). Polydopamine (PDA) was selected as the polymeric carbon precursor because of the presence of many amine groups in its structure. This high percentage of nitrogen leaves a nitrogen-doped carbon layer, which substantially improves the electrical conductivity of the coated material [47–49]. The hard template was etched with 2 M HCl aqueous solution and the remaining N-HCNR was introduced to molten sulfur (S@HCNR). In the final step, a thin uniform layer of MnO_2 was formed around the nanorods (S@HCNR@MnO_2).

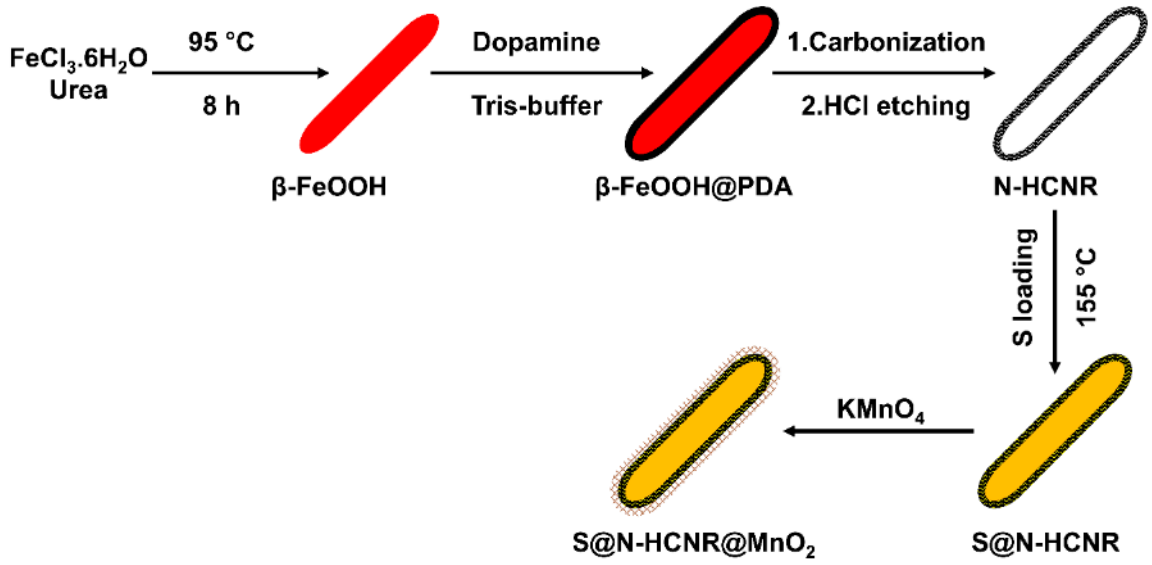

Figure 1. Schematic illustration of the synthesis steps of S@HCNR@MnO_2 nanorods.

Figures 2 and 3 contain the SEM micrographs and EDXA elemental spectra of the nanorods at different stages of synthesis. The hydrolysis of $FeCl_3$ in the presence of urea at 90 °C resulted in the formation of spindle-like β-FeOOH nanorods with uniform size distribution (Figure 2a). After polymerization of dopamine and further carbonization, β-FeOOH oxidized to Fe_3O_4 core with a nitrogen-doped carbon shell, Fe_3O_4@N-C. The strong binding affinity of polydopamine to the iron oxide core provoked the evolution of a uniform carbon layer, derived from polydopamine, after heat treatment at 500 °C (Figure 2b) [50]. Next, the Fe_3O_4 template was completely dissolved by HCl aqueous solution and hollow nitrogen-doped carbon nanorods (N-HCNRs) remained (Figures 2c and 3a). Both ends of the carbon nanorods were slightly smaller than the middle core. The N-HCNRs maintained the spindle morphology, with lengths of 1–1.5 μm and diameters ranging from 150 to 200 nm. This unique structure makes them excellent hosts for sulfur. The sublimed sulfur was melted at 155 °C and diffused into the host inside the autoclave to obtain S@HCNRs (Figure 2d). This is confirmed by the presence of strong elemental sulfur peaks in the EDX spectrum (Figure 3b). It is important to note that the EDX spectra for each specimen were collected at different spots in order to generate more reliable data. Figure 3c clearly indicates the presence of Mn in the final structure, S@NHCNR@MnO_2. In the final step, the δ-MnO_2 was formed on the surface of S@HCNR with the aid of the reduction of $KMnO_4$ in the presence of both sulfur and carbon (Equations (1) and (2)). The MnO_2 layer wrapped the sulfur-filled nanorods conformally without causing any change in their size or morphology (Figure 2e). The elemental manganese peaks originated from the MnO_2 shell (Figure 3c).

$$6KMnO_4 + 3S + H_2O = 6MnO_2 + K_2SO_4 + K_3H(SO_4)_2 + KOH \quad (1)$$

$$4KMnO_4 + 3C + H_2O = 4MnO_2 + 2KHCO_3 + K_2CO_3 \quad (2)$$

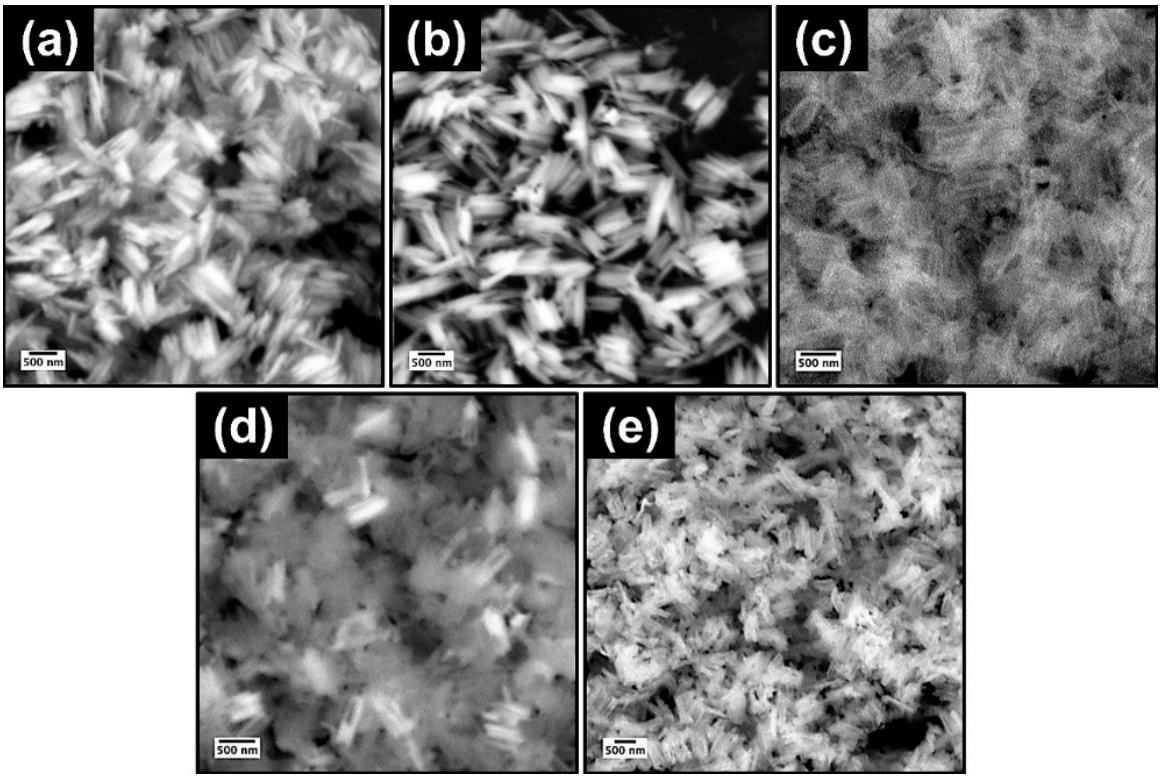

Figure 2. SEM images of (**a**) β-FeOOH, (**b**) Fe_3O_4@N-C, (**c**) N-HCNR, (**d**) S@HCNR, and (**e**) S@HCNR@MnO_2.

The porous structure of N-HCNR was evaluated by the nitrogen adsorption–desorption technique. Both adsorption and desorption isotherms are plotted in Figure 4. These isotherms were identified as type IV isotherms with type III hysteresis. We consider this is the most important structure for BET analysis, because the information (surface area, pore diameter and pore volume) we get is directly related to sulfur loading. The calculated Brunauer–Emmett–Teller (BET) surface area at 77 K was 509 m^2 g^{-1}, while a pore volume and pore diameter of 0.251 cm^3 g^{-1} and 3 nm were computed by Barrett−Joyner−Halenda (BJH) analysis, respectively. The relatively high surface area and pore volume of the N-HCNR makes it a strong host candidate for sulfur loading. We did not perform BET analysis of the follow-up structures, S@N-HCNR and S@N-HCNR@MnO_2, because the results will not be informative, as all voids will be filled up with sulfur after the loading of sulfur/MnO_2 coating.

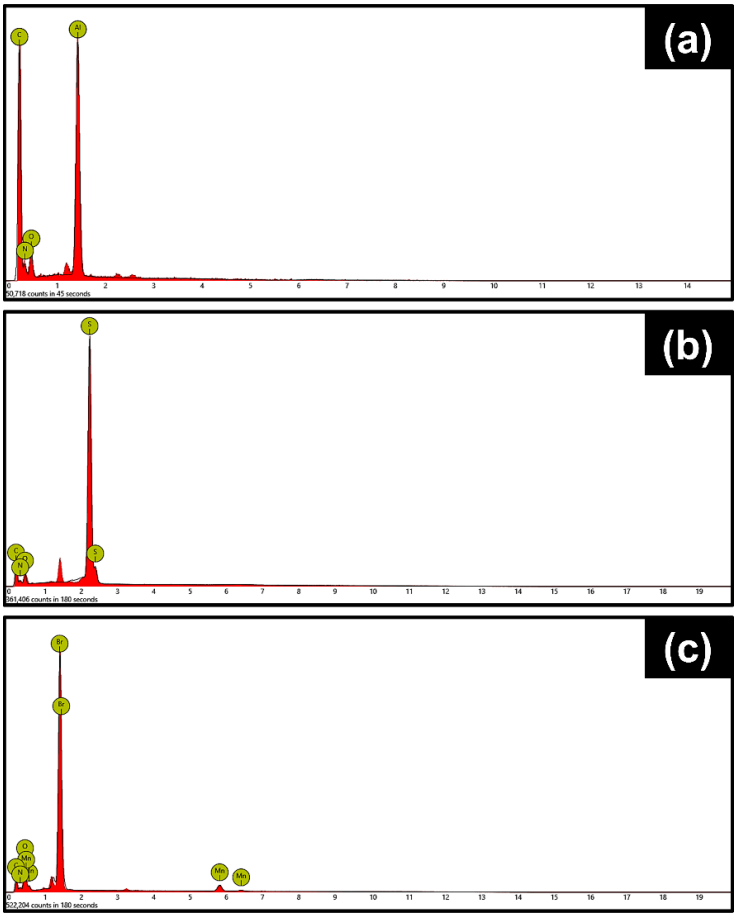

Figure 3. Energy-dispersive X-ray (EDX) spectra of (**a**) N-HCNR, (**b**) S@HCNR, and (**c**) HCNR@MnO_2.

The electrochemical performance of the both S@HCNR and S@HCNR@MnO_2 nanorods were investigated in half-cell with Li chip as both counter and reference electrode. The reported capacities were normalized based on the sulfur content of each sample. S@HCNR was compromised of about 70 wt.% of sulfur, while S@HCNR@MnO_2 nanorods contained 60 wt.% of sulfur and 10 wt.% of MnO_2. The charge–discharge behavior of the electrode material was evaluated at a 0.2C rate (1C = 1675 mA h g^{-1}) in the voltage window of 1.7–2.8 V vs. Li^+/Li (Figure 5a). The S@HCNR@MnO_2 nanorods delivered an excellent initial discharge capacity of 1661 mA h g^{-1}, while, after 70 cycles, the capacity decayed to 1342 mA h g^{-1} with a Coulombic efficiency of 99%. This translates to an ~80% capacity retention. After the first cycle, the discharge capacity decreased to 1500 mA h g^{-1} and then the cell stabilized with a slow decay rate. Typical galvanostatic discharge–charge profiles of S@HCNR@MnO_2 electrodes for different cycles at 0.2C are shown in Figure 5b. It is worth noting that, during the first charge, the voltage reached 2.3 V and then dropped to 2.2 V. This hump is due to the MnO_2 coating layer, which leads to the increase in the charge resistance [45,51]. The height of this hump decreased in the successive cycles. Furthermore, no plateau related to the reaction of lithium with MnO_2 shell was detected in the voltage window of 1.7–2.8 V [52,53]. Consecutive cycling performance of the S@HCNR and S@HCNR@MnO_2 nanorods with gradual increase in current densities for every 10 cycles are shown in Figure 5c. The rate was increased from 0.2C to 2C, followed by a recovery at 0.2C. The S@HCNR@MnO_2 electrode delivered initial specific capacity of 1641 mA h g^{-1} at 0.2C without any noticeable overpotential, which is ~98% of the theoretical specific capacity of sulfur. As the C-rate increased to 0.5C, 1C and 2C, the specific discharge capacity was gradually reduced to 1300 mA h g^{-1}, 400 mA h g^{-1} and 320 mA h g^{-1}, respectively. When the current rate was switched back to 0.2C, the discharge capacity was recovered to ~1350 mA h g^{-1}, which is close to the delivered capacity

recorded at 0.2C in the first cycle. In comparison, the discharge capacity of the S@HCNR nanorods decreased more significantly with the increase in charging/discharging rates; the specific capacity at initial cycle at 0.2C was 1300 mA h g^{-1}, but it declined to 220 mA h g^{-1} at 2C. This demonstrates the excellent rate capability of S@HCNR@MnO_2. To further understand the kinetics of the redox reactions, the voltage profiles of S@HCNR@MnO_2 cathodes between 1.7 and 2.8 V (vs. Li^+/Li) at different current rates are presented in Figure 5d. Two voltage plateaus at 2.3 and 2.0 V are associated with the formation of long- and short-chain LiPSs, respectively [54]. No peaks or shoulders related to the intercalation of Li^+ ion to MnO_2 were observed. The good electrochemical properties of the S@HCNR@MnO_2 hybrid cathode are related to the engineered design of the spindle-like nanorods. The inner carbon layer is in close contact with the sulfur and helps to improve the electrical conductivity. The outer MnO_2 layer serves as the protective layer against the polysulfide shuttling effect and partially increases the overall conductivity of the nanorod structure. Although the electrochemical performance of the nanorods is good, the capacity drop from 0.5C to 1C was very serious. In fact, the capacity drop at higher rates is a common problem in Li-S battery technology. Several other groups have also pointed out this big capacity drop at high-rate charge/discharge [41,43,53]. It is mainly related to the slow lithiation/delithiation reaction kinetics and poor Li^+ ion diffusion through the cathode active materials at higher rates. The huge volume change of sulfur during the initial cycles can cause some cracks in the carbon host structure, which in successive cycles can promote the leakage of LiPSs. Additionally, the presence of some un-infiltrated sulfur on the surface of the S@HCNR@MnO_2 electrode can have negative effects on the electrode performance, since these free sulfur particles can undergo redox reactions in a different way than that of the encapsulated ones. Even with the huge capacity decay at higher current densities, the S@HCNR@MnO_2 electrode showed superior discharge capacities compared to the S@HCNR electrode. Finally, the delivered discharge capacity and rate performance of the S@HCNR@MnO_2 was superior to MnO_2-coated sulfur-filled hollow carbon nanospheres (S@HCN@MnO_2) [55]. This is due to better utilization of sulfur during the charge/discharge process in the hollow nanorod structure compared to the hollow nanospheres. Moreover, the physical and chemical confinement of sulfur/LiPSs can be better achieved in the hollow nanorod design. Furthermore, the sulfur is in better contact with the carbon layer in nanorods, which simply translates to higher sulfur utilization [39,40,43,52,54].

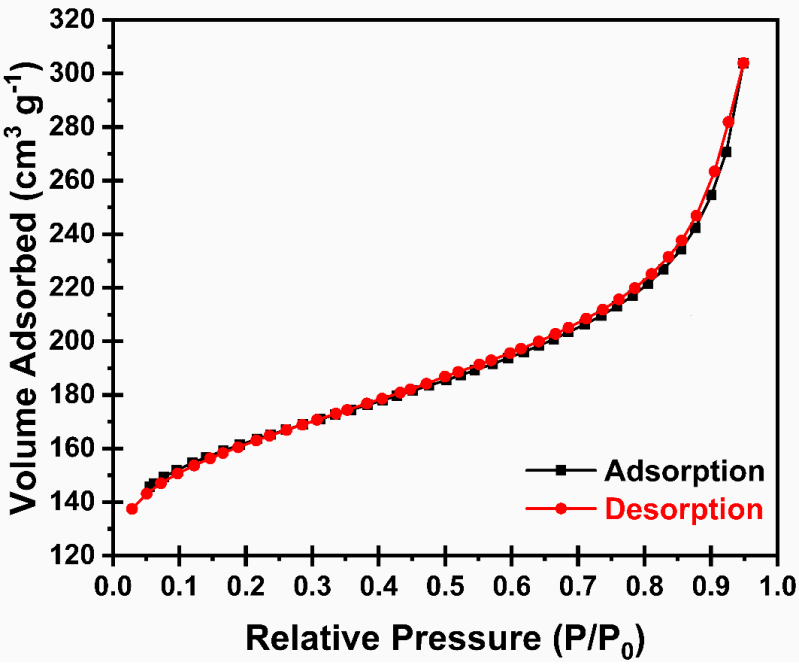

Figure 4. Nitrogen adsorption–desorption isotherms for HCNR.

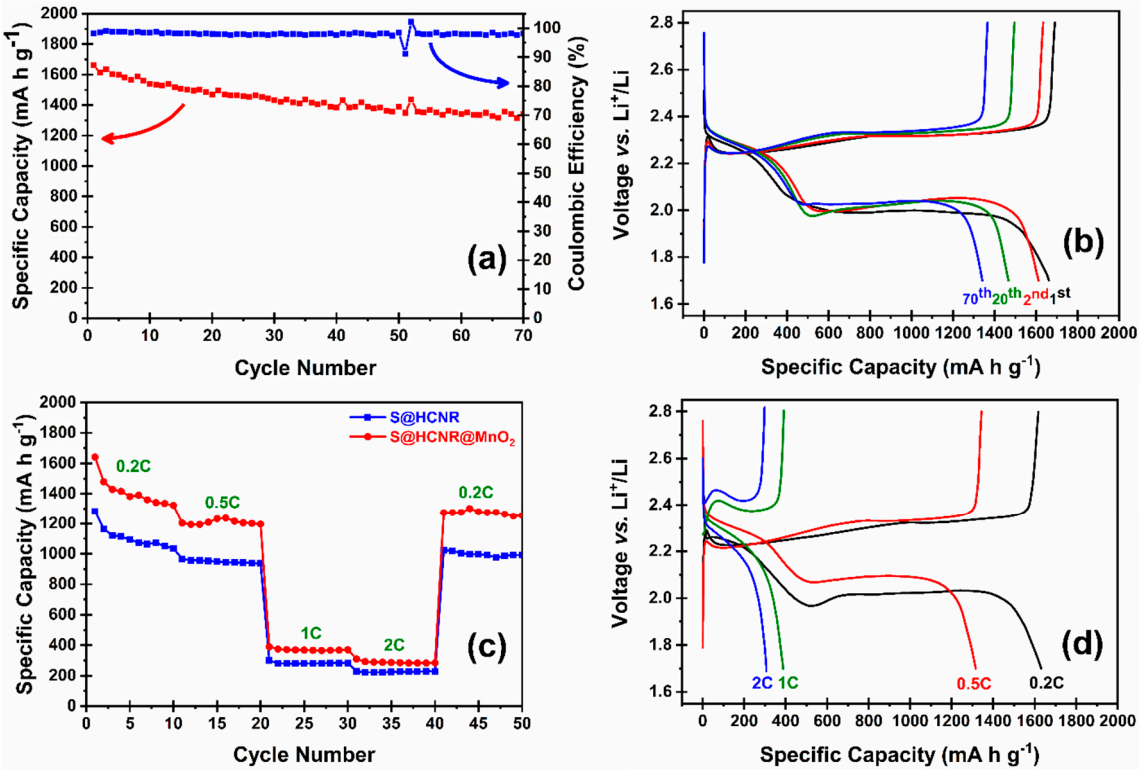

Figure 5. (**a**) Cycling performance and Coulombic efficiency of S@HCNR@MnO_2 electrode at a current rate of 0.2C, (**b**) voltage profiles of the S@HCS@MnO_2 composite electrode at 0.2C, (**c**) comparison between rate performances of S@HCNR@MnO_2 and S@HCNR nanorods at different charge/discharge rates, and (**d**) first charge–discharge profiles of the S@HCS@MnO_2 cathode at different C-rates.

4. Conclusions

In summary, we have synthesized dual core–shell-structured S@HCNR@MnO_2 spindle-like nanorods as a promising cathode material for lithium–sulfur batteries. The nitrogen-doped hollow carbon nanorods with a diameter of less than 200 nm and length of 1–2 µm act as a host for the sulfur material. The cathode delivered an excellent initial discharge capacity of 1661 mA h g^{-1} and capacity retention of above 80% after 70 cycles at a 0.2C rate. The enhanced performance of S@HCNR@MnO_2 is attributed to several factors. First, N-doped hollow carbon nanorods not only enhance the electrical conductivity of the cathode, but also facilitate chemical binding with polysulfide intermediate products. Second, the hollow structure can accommodate volumetric expansion of sulfur upon lithiation and possesses physical encapsulation of polysulfide in the cathode structure design. Third, the formation of one-dimensional (1D) structure (linear electron conduction path) facilitates fast ion and electron transport. Finally, the polar MnO_2 shell, with the ability to form strong chemical bonding with polysulfides, minimizes polysulfide shuttle effect in the cell. Although the results obtained in this study were promising, further optimizations are required to achieve a robust sulfur nanocomposite with better rate capability and higher delivered capacities. The carbon framework can be prepared from other carbon sources such as polyacrylonitrile (PAN) with different pore size distribution. The MnO_2 layer thickness needs to be adjusted to achieve maximum protection against sulfur/polysulfides leakage. It is also worth testing this nanocomposite with separators coated with polysulfide barrier materials, such as In_2O_3 [33] and AlF_3 [56].

Author Contributions: H.D. (Conceptualization, Methodology, Writing original draft); M.A. (Data curation, Investigation, Writing, review & editing); D.A. (Writing, review & editing, Software, Data curation, Visualization); Z.Y. (Software, Methodology, Data curation); K.K. (Data curation, Visualization, Investigation); C.U.S. (Supervision, Writing—review & editing); B.K.M. (Conceptualization, Methodology, Supervision, Writing, review & editing). All authors have read and agree to the published version of the manuscript.

Funding: We thank the Wanger Institute for Sustainable Energy Research (WISER# 6-1-17) Foundation for the partial financial support of this research work.

Conflicts of Interest: The authors declare no conflicts of interest.

References

1. Hoffert, M.I.; Caldeira, K.; Benford, G.; Criswell, D.R.; Green, C.; Herzog, H.; Jain, A.K.; Kheshgi, H.S.; Lackner, K.S.; Lewis, J.S.; et al. Advanced technology paths to global climate stability: Energy for a greenhouse planet. *Science* **2002**, *298*, 981–987. [CrossRef] [PubMed]
2. Tarascon, J.M.; Armand, M. Issues and challenges facing rechargeable lithium batteries. *Nature* **2001**, *414*, 359–367. [CrossRef] [PubMed]
3. Armand, M.; Tarascon, J.M. Building better batteries. *Nature* **2008**, *451*, 652–657. [CrossRef] [PubMed]
4. Lin, Z.; Liang, C. Lithium-sulfur batteries: From liquid to solid cells. *J. Mater. Chem. A* **2015**, *3*, 936–958. [CrossRef]
5. Rosenman, A.; Markevich, E.; Salitra, G.; Aurbach, D.; Garsuch, A.; Chesneau, F.F. Review on Li-sulfur battery systems: An integral perspective. *Adv. Energy Mater.* **2015**, *5*, 1500212. [CrossRef]
6. Barghamadi, M.; Kapoor, A.; Wen, C. A review on Li-S batteries as a high efficiency rechargeable lithium battery. *J. Electrochem. Soc.* **2013**, *160*, A1256–A1263. [CrossRef]
7. Zhang, X.; Xie, H.; Kim, C.S.; Zaghib, K.; Mauger, A.; Julien, C.M. Advances in lithium-sulfur batteries. *Mater. Sci. Eng. R Rep.* **2017**, *121*, 1–29. [CrossRef]
8. Ji, X.; Nazar, L.F. Advances in Li–S batteries. *J. Mater. Chem.* **2010**, *20*, 9821–9826. [CrossRef]
9. Manthiram, A.; Fu, Y.; Su, Y.-S. Challenges and prospects of lithium-sulfur batteries. *Acc. Chem. Res.* **2013**, *46*, 1125–1134. [CrossRef]
10. Yang, Y.; Zheng, G.; Cui, Y. Nanostructured sulfur cathodes. *Chem. Soc. Rev.* **2013**, *42*, 3018–3032. [CrossRef]
11. Chen, L.; Shaw, L.L. Recent advances in lithium-sulfur batteries. *J. Power Sources* **2014**, *267*, 770–783. [CrossRef]
12. Chen, L.; Liu, Y.; Ashuri, M.; Liu, C.; Shaw, L.L. Li_2S encapsulated by nitrogen-doped carbon for lithium sulfur batteries. *J. Mater. Chem. A* **2014**, *2*, 18026–18032. [CrossRef]
13. Kumar, R.; Liu, J.; Hwang, J.-Y.; Sun, Y.-K. Recent research trends in Li-S batteries. *J. Mater. Chem. A* **2018**, *6*, 11582–11605. [CrossRef]
14. Manthiram, A.; Fu, Y.; Chung, S.-H.; Zu, C.; Su, Y.-S. Rechargeable lithium-sulfur batteries. *Chem. Rev.* **2014**, *114*, 11751–11787. [CrossRef] [PubMed]
15. Schuster, J.; He, G.; Mandlmeier, B.; Yim, T.; Lee, K.T.; Bein, T.; Nazar, L.F. Spherical ordered mesoporous carbon nanoparticles with high porosity for lithium-sulfur batteries. *Angew. Chem. Int. Ed.* **2012**, *51*, 3591–3595. [CrossRef]
16. Borchardt, L.; Oschatz, M.; Kaskel, S. Carbon materials for lithium sulfur batteries—Ten critical questions. *Chem. A Eur. J.* **2016**, *22*, 7324–7351. [CrossRef]
17. Chen, S.; Sun, B.; Xie, X.; Mondal, A.K.; Huang, X.; Wang, G. Multi-chambered micro/mesoporous carbon nanocubes as new polysulfides reserviors for lithium–sulfur batteries with long cycle life. *Nano Energy* **2015**, *16*, 268–280. [CrossRef]
18. Li, G.; Sun, J.; Hou, W.; Jiang, S.; Huang, Y.; Geng, J. Three-dimensional porous carbon composites containing high sulfur nanoparticle content for high-performance lithium-sulfur batteries. *Nat. Commun.* **2016**, *7*, 10601. [CrossRef]
19. Yuan, L.; Yuan, H.; Qiu, X.; Chen, L.; Zhu, W. Improvement of cycle property of sulfur-coated multi-walled carbon nanotubes composite cathode for lithium/sulfur batteries. *J. Power Sources* **2009**, *189*, 1141–1146. [CrossRef]
20. Dörfler, S.; Hagen, M.; Althues, H.; Tübke, J.; Kaskel, S.; Hoffmann, M.J. High capacity vertical aligned carbon nanotube/sulfur composite cathodes for lithium-sulfur batteries. *Chem. Commun.* **2012**, *48*, 4097–4099. [CrossRef]

21. Sun, L.; Wang, D.; Luo, Y.; Wang, K.; Kong, W.; Wu, Y.; Zhang, L.; Jiang, K.; Li, Q.; Zhang, Y.; et al. Sulfur embedded in a mesoporous carbon nanotube network as a binder-free electrode for high-performance lithium-sulfur batteries. *ACS Nano* **2016**, *10*, 1300–1308. [CrossRef]
22. Papandrea, B.; Xu, X.; Xu, Y.; Chen, C.-Y.; Lin, Z.; Wang, G.; Luo, Y.; Liu, M.; Huang, Y.; Mai, L.; et al. Three-dimensional graphene framework with ultra-high sulfur content for a robust lithium-sulfur battery. *Nano Res.* **2016**, *9*, 240–248. [CrossRef]
23. Wang, J.-Z.; Lu, L.; Choucair, M.; Stride, J.A.; Xu, X.; Liu, H.-K. Sulfur-graphene composite for rechargeable lithium batteries. *J. Power Sources* **2011**, *196*, 7030–7034. [CrossRef]
24. Liu, Y.; Wang, X.; Dong, Y.; Tang, Y.; Wang, L.; Jia, D.; Zhao, Z.; Qiu, J. Self-assembled sulfur/reduced graphene oxide nanoribbon paper as a free-standing electrode for high performance lithium-sulfur batteries. *Chem. Commun.* **2016**, *52*, 12825–12828. [CrossRef] [PubMed]
25. Zheng, Z.; Guo, H.; Pei, F.; Zhang, X.; Chen, X.; Fang, X.; Wang, T.; Zheng, N. High sulfur loading in hierarchical porous carbon rods constructed by vertically oriented porous graphene-like nanosheets for Li-S batteries. *Adv. Funct. Mater.* **2016**, *26*, 8952–8959. [CrossRef]
26. Hu, G.; Xu, C.; Sun, Z.; Wang, S.; Cheng, H.-M.; Li, F.; Ren, W. 3D graphene-foam–reduced-graphene-oxide hybrid nested hierarchical networks for high-performance Li–S batteries. *Adv. Mater.* **2016**, *28*, 1603–1609. [CrossRef]
27. Ji, L.; Rao, M.; Zheng, H.; Zhang, L.; Li, Y.; Duan, W.; Guo, J.; Cairns, E.J.; Zhang, Y. Graphene oxide as a sulfur immobilizer in high performance lithium/sulfur cells. *J. Am. Chem. Soc.* **2011**, *133*, 18522–18525. [CrossRef]
28. Wang, D.-W.; Zeng, Q.; Zhou, G.; Yin, L.; Li, F.; Cheng, H.-M.; Gentle, I.R.; Lu, G.Q.M. Carbon-sulfur composites for Li-S batteries: Status and prospects. *J. Mater. Chem. A* **2013**, *1*, 9382–9394. [CrossRef]
29. Ma, L.; Hendrickson, K.E.; Wei, S.; Archer, L.A. Nanomaterials: Science and applications in the lithium-sulfur battery. *Nano Today* **2015**, *10*, 315–338. [CrossRef]
30. Luo, Z.; Lei, W.; Wang, X.; Pan, J.; Pan, Y.; Xia, S. AlF3 coating as sulfur immobilizers in cathode material for high performance lithium-sulfur batteries. *J. Alloys Compd.* **2020**, *812*, 152132. [CrossRef]
31. Dharmasena, R.; Thapa, A.K.; Hona, R.K.; Jasinski, J.; Sunkara, M.K.; Sumanasekera, G.U. Mesoporous TiO_2 coating on carbon-sulfur cathode for high capacity Li-sulfur battery. *RSC Adv.* **2018**, *8*, 11622–11632. [CrossRef]
32. Ashuri, M.; Dunya, H.; Yue, Z.; Alramahi, D.; Mei, X.; Kucuk, K.; Aryal, S.; Segre, C.U.; Mandal, B.K. Enhancement in electrochemical performance of lithium-sulfur cells through sulfur encapsulation in hollow carbon nanospheres coated with ultra-thin aluminum fluoride layer. *ChemistrySelect* **2019**, *4*, 12622–12629. [CrossRef]
33. Yang, X.; Qian, X.; Jin, L.; Yao, S.; Rao, D.; Shen, X.; Wang, L.; Tan, J. Separator modified with Ketjenblack-In_2O_3 nanoparticles for long cycle-life lithium-sulfur batteries. *J. Solid State Electrochem.* **2019**, *23*, 645–656. [CrossRef]
34. Wu, D.S.; Shi, F.; Zhou, G.; Zu, C.; Liu, C.; Liu, K.; Liu, Y.; Wang, J.; Peng, Y.; Cui, Y. Quantitative investigation of polysulfide adsorption capability of candidate materials for Li-S batteries. *Energy Storage Mater.* **2018**, *13*, 241–246. [CrossRef]
35. Zhang, G.; Zhang, Z.-W.; Peng, H.-J.; Huang, J.-Q.; Zhang, Q. A toolbox for lithium–sulfur battery research: Methods and protocols. *Small Methods* **2017**, *1*, 1700134. [CrossRef]
36. Song, M.-K.; Cairns, E.J.; Zhang, Y. Lithium/sulfur batteries with high specific energy: Old challenges and new opportunities. *Nanoscale* **2013**, *5*, 2186–2204. [CrossRef]
37. Akridge, J.R.; Mikhaylik, Y.V.; White, N. Li/S fundamental chemistry and application to high-performance rechargeable batteries. *Solid State Ion.* **2004**, *175*, 243–245. [CrossRef]
38. Dunya, H.; Yue, Z.; Ashuri, M.; Mei, X.; Lin, Y.; Kucuk, K.; Aryal, S.; Segre, C.U.; Mandal, B.K. A new graphitic carbon nitride-coated dual core–shell sulfur cathode for highly stable lithium-sulfur cells. *Mater. Chem. Phys.* **2020**, *246*, 122842. [CrossRef]
39. Huang, X.; Shi, K.; Yang, J.; Mao, G.; Chen, J. MnO_2-GO double-shelled sulfur (S@MnO_2@GO) as a cathode for Li-S batteries with improved rate capability and cyclic performance. *J. Power Sources* **2017**, *356*, 72–79. [CrossRef]

40. Ni, L.; Zhao, G.; Wang, Y.; Wu, Z.; Wang, W.; Liao, Y.; Yang, G.; Diao, G. Coaxial carbon/MnO_2 hollow nanofibers as sulfur hosts for high-performance lithium-sulfur batteries. *Chem. Asian J.* **2017**, *12*, 3128–3134. [CrossRef]
41. Lee, J.; Hwang, T.; Lee, Y.; Lee, J.K.; Choi, W. Coating of sulfur particles with manganese oxide nanowires as a cathode material in lithium-sulfur batteries. *Mater. Lett.* **2015**, *158*, 132–135. [CrossRef]
42. Sun, W.; Ou, X.; Yue, X.; Yang, Y.; Wang, Z.; Rooney, D.; Sun, K. A simply effective double-coating cathode with MnO_2 nanosheets/graphene as functionalized interlayer for high performance lithium-sulfur batteries. *Electrochim. Acta* **2016**, *207*, 198–206. [CrossRef]
43. Li, Z. MnO_2-graphene nanosheets wrapped mesoporous carbon/sulfur composite for lithium-sulfur batteries. *R. Soc. Open Sci.* **2018**, *5*, 171824. [CrossRef] [PubMed]
44. Liang, X.; Hart, C.; Pang, Q.; Garsuch, A.; Weiss, T.; Nazar, L.F. A highly efficient polysulfide mediator for lithium–sulfur batteries. *Nat. Commun.* **2015**, *6*, 5682. [CrossRef] [PubMed]
45. Liang, X.; Nazar, L.F. *In Situ* reactive assembly of scalable core-shell sulfur-MnO_2 composite cathodes. *ACS Nano* **2016**, *10*, 4192–4198. [CrossRef]
46. Qian, C.; Guo, P.; Zhang, X.; Zhao, R.; Wu, Q.; Huan, L.; Shen, X.; Chen, M. Nitrogen-doped mesoporous hollow carbon nanoflowers as high performance anode materials of lithium ion batteries. *RSC Adv.* **2016**, *6*, 93519–93524. [CrossRef]
47. Zhou, W.; Xiao, X.; Cai, M.; Yang, L. Polydopamine-coated, nitrogen-doped, hollow carbon-sulfur double-layered core-shell structure for improving lithium-sulfur batteries. *Nano Lett.* **2014**, *14*, 5250–5256. [CrossRef]
48. Kong, J.; Yee, W.A.; Yang, L.; Wei, Y.; Phua, S.L.; Ong, H.G.; Ang, J.M.; Li, X.; Lu, X. Highly electrically conductive layered carbon derived from polydopamine and its functions in SnO_2-based lithium ion battery anodes. *Chem. Commun.* **2012**, *48*, 10316–10318. [CrossRef]
49. Ashuri, M.; He, Q.; Liu, Y.; Shaw, L.L. Investigation towards scalable processing of silicon/graphite nanocomposite anodes with good cycle stability and specific capacity. *Nano Mater. Sci.* **2019**. [CrossRef]
50. Chen, M.; Jiang, J.; Zhou, X.; Diao, G. Preparation of akaganeite nanorods and their transformation to sphere shape hematite. *J. Nanosci. Nanotechnol.* **2008**, *8*, 3942–3948. [CrossRef]
51. Liu, J.; Wang, C.; Liu, B.; Ke, X.; Liu, L.; Shi, Z.; Zhang, H.; Guo, Z. Rational synthesis of MnO_2@CMK/S composite as cathode materials for lithium-sulfur batteries. *Mater. Lett.* **2017**, *195*, 236–239. [CrossRef]
52. Ni, L.; Wu, Z.; Zhao, G.; Sun, C.; Zhou, C.; Gong, X.; Diao, G. Core-shell structure and interaction mechanism of γ-MnO_2 coated sulfur for improved lithium-sulfur batteries. *Small* **2017**, *13*, 1603466. [CrossRef] [PubMed]
53. Wang, S.; Yang, Z.; Zhang, H.; Tan, H.; Yu, J.; Wu, J. Mesoporous β-MnO_2/sulfur composite as cathode material for Li-S batteries. *Electrochim. Acta* **2013**, *106*, 307–311. [CrossRef]
54. Ni, L.; Zhao, G.; Yang, G.; Niu, G.; Chen, M.; Diao, G. Dual Core-shell-structured S@C@MnO_2 nanocomposite for highly stable lithium-sulfur batteries. *ACS Appl. Mater. Interfaces* **2017**, *9*, 34793–34803. [CrossRef]
55. Yue, Z.; Dunya, H.; Kucuk, K.; Aryal, S.; Ma, Q.; Antonov, S.; Ashuri, M.; Alabbad, B.; Lin, Y.; Segre, C.U.; et al. MnO_2-coated sulfur-filled hollow carbon nanosphere-based cathode materials for enhancing electrochemical performance of Li-S cells. *J. Electrochem. Soc.* **2019**, *166*, A1355–A1362. [CrossRef]
56. Bugga, R.; Jones, J.-P.; Jones, S.C.; Krause, F.C.; Pasalic, J.; Ganapathi, D.S.; Hendrickson, M.; Plichta, E.J. New separators in lithium/sulfur cells with high-capacity cathodes. *J. Electrochem. Soc.* **2018**, *165*, A6021–A6028. [CrossRef]